STEM CELLS TRANSLATIONAL MEDICINE®

TISSUE ENGINEERING AND REGENERATIVE MEDICINE

Priming Dental Pulp Stem Cells With Fibroblast Growth Factor-2 Increases Angiogenesis of Implanted Tissue-Engineered Constructs Through Hepatocyte Growth Factor and Vascular Endothelial Growth Factor Secretion

CAROLINE GORIN,[a,b,*] GAEL Y. ROCHEFORT,[a,*] RUMEYZA BASCETIN,[c,d,e] HANRU YING,[c,d,e] JULIE LESIEUR,[a] JÉRÉMY SADOINE,[a] NATHAN BECKOUCHE,[c,d,e] SARAH BERNDT,[c,d,e] ANITA NOVAIS,[a] MATTHIEU LESAGE,[c,d,e] BENOIT HOSTEN,[f] LAETITIA VERCELLINO,[g] PASCAL MERLET,[g] DOMINIQUE LE-DENMAT,[a] CARMEN MARCHIOL,[h] DIDIER LETOURNEUR,[i] ANTONINO NICOLETTI,[i] SIBYLLE OPSAHL VITAL,[a,b] ANNE POLIARD,[a] BENJAMIN SALMON,[a,b] LAURENT MULLER,[c,d,e] CATHERINE CHAUSSAIN,[a,b,†] STÉPHANE GERMAIN[c,d,e,†]

[a]EA 2496 Pathologies, Imagerie et Biothérapies orofaciales et Plateforme Imagerie du Vivant, Dental School, Université Paris Descartes Sorbonne Paris Cité, Montrouge, France; [b]Assistance Publique des Hôpitaux de Paris (AP-HP) Département d'Odontologie, Hôpitaux Universitaires PNVS, Paris, France; [c]Center for Interdisciplinary Research in Biology, Collège de France, Paris, France; [d]Inserm U1050, Paris, France; [e]CNRS UMRS 7241, Paris, France; [f]INSERM UMR-S1144, Université Paris Descartes-Paris Diderot Sorbonne Paris Cité, AP-HP, Hôpital St. Louis, Unité Claude Kellershohn, Paris, France; [g]Université Paris Diderot, AP-HP, Hôpital St. Louis, Unité Claude Kellershohn, Paris, France; [h]Institut Cochin, Plateforme Imagerie du vivant, Université Paris Descartes Sorbonne Paris Cité, Paris, France; [i]INSERM U1148, Laboratory of Vascular Translational Science, Université Paris Diderot Sorbonne Paris Cité, Sorbonne Paris Cité, Faculté de Médecine, Site Xavier Bichat, and Département Hospitalo-Universitaire Fibrosis, Inflammation, and Remodeling, Paris, France

[*]Contributed equally.

[†]Co-senior authors.

Correspondence: Catherine Chaussain, Ph.D., Dental School, Université Paris Descartes Sorbonne Paris Cité, 1 rue Maurice Arnoux 92120 Montrouge, France. Telephone: 331-5807-6724; E-Mail: catherine.chaussain@parisdescartes.fr; or Laurent Muller, Ph.D., Collège de France, Center for Interdisciplinary Research in Biology, 11 Place Marcelin Berthelot, Paris 75005, France. Telephone: 331-4427-1429; E-Mail: laurent.muller@college-de-france.fr

Received July 22, 2015; accepted for publication October 7, 2015; published Online First on January 21, 2016.

1066-5099/2016/$20.00/0

http://dx.doi.org/10.5966/sctm.2015-0166

Key Words. Pulp engineering • Mesenchymal stem cells • Hypoxia • Angiogenesis • Dynamic vascular imaging • Vascular endothelial growth factor • Hepatocyte growth factor

ABSTRACT

Tissue engineering strategies based on implanting cellularized biomaterials are promising therapeutic approaches for the reconstruction of large tissue defects. A major hurdle for the reliable establishment of such therapeutic approaches is the lack of rapid blood perfusion of the tissue construct to provide oxygen and nutrients. Numerous sources of mesenchymal stem cells (MSCs) displaying angiogenic potential have been characterized in the past years, including the adult dental pulp. Establishment of efficient strategies for improving angiogenesis in tissue constructs is nevertheless still an important challenge. Hypoxia was proposed as a priming treatment owing to its capacity to enhance the angiogenic potential of stem cells through vascular endothelial growth factor (VEGF) release. The present study aimed to characterize additional key factors regulating the angiogenic capacity of such MSCs, namely, dental pulp stem cells derived from deciduous teeth (SHED). We identified fibroblast growth factor-2 (FGF-2) as a potent inducer of the release of VEGF and hepatocyte growth factor (HGF) by SHED. We found that FGF-2 limited hypoxia-induced downregulation of HGF release. Using three-dimensional culture models of angiogenesis, we demonstrated that VEGF and HGF were both responsible for the high angiogenic potential of SHED through direct targeting of endothelial cells. In addition, FGF-2 treatment increased the fraction of Stro-1+/CD146+ progenitor cells. We then applied in vitro FGF-2 priming to SHED before encapsulation in hydrogels and in vivo subcutaneous implantation. Our results showed that FGF-2 priming is more efficient than hypoxia at increasing SHED-induced vascularization compared with nonprimed controls. Altogether, these data demonstrate that FGF-2 priming enhances the angiogenic potential of SHED through the secretion of both HGF and VEGF. STEM CELLS TRANSLATIONAL MEDICINE *2016;5:392–404*

SIGNIFICANCE

The results from the present study show that fibroblast growth factor-2 (FGF-2) priming is more efficient than hypoxia at increasing dental pulp stem cells derived from deciduous teeth (SHED)-induced vascularization compared with nonprimed controls. Together, these data demonstrate that FGF-2 priming enhances the angiogenic potential of SHED through the secretion of both hepatocyte growth factor and vascular endothelial growth factor.

INTRODUCTION

The delivery of tissue constructs seeded with adult stem cells into injured and ischemic tissues has been emerging as a potential therapeutic option for tissue repair and regeneration. The success of this regenerative strategy is directly conditioned by the establishment of a fully functional vascular network within the tissue-engineered constructs. The blood supply must be quickly established

to provide oxygen and nutrients and to prevent necrosis. Identifying stem or progenitor cell populations able to both participate in tissue regeneration and promote angiogenesis is therefore essential for developing such novel tissue regeneration strategies [1]. Dental pulp mesenchymal stem cells (DPSCs) have been described as a potential alternative for tissue engineering, because of their extended potential for proliferation and differentiation and their paracrine properties [2–6]. We have recently shown that implantation of a tissue construct composed of rat DPSCs seeded in a three-dimensional (3D) collagen hydrogel into the emptied pulp chamber of a rat molar was capable of generating a vascularized pulp-like tissue [7]. Creating a functional vasculature represents one of the most fundamental challenges in tissue engineering. Therefore, understanding the mechanisms that regulate angiogenesis in this context is critical. Bone marrow-derived stem cells (BMSCs) and adipose-derived stem cells (ASCs) have been shown to induce vessel formation [8–11]. Likewise, DPSCs display strong proangiogenic properties [12–14] that remain to be fully understood. DPSCs are more efficient at vessel formation than other mesenchymal stem cells from the tooth organ or BMSCs [15, 16], further supporting their clinical interest. DPSCs have been involved in the promotion of angiogenesis through either secretion of proangiogenic factors or differentiation into endothelial cells (ECs) [12–14, 17]. Several lines of evidence, however, support that their paracrine effect is the main mechanism involved: (a) the long treatments (3–4 weeks) described for cell differentiation in vitro are not compatible with the requirement for rapid angiogenesis [18]; (b) conflicting results have been reported concerning differentiation into ECs in vivo [12, 19, 20]; and (c) low rates of cell insertion in the endothelium have been observed in vivo [21].

The tissue remodeling that accompanies successful tissue engineering therapy is regulated by growth factors, cytokines, components of the extracellular matrix, and/or oxygen tension, which target ECs [22, 23]. The grafting environment is poor in oxygen, and hypoxia is a major stimulus for angiogenesis through the induction of vasodilatation, proliferation, and migration of ECs. Activation of the hypoxia inducible factor (HIF) pathway triggers transcription of a wide panel of genes, including angiogenic factors such as vascular endothelial growth factor (VEGF) and extracellular matrix (ECM) components [24–26]. Recent works have identified VEGF as the major factor responsible for the proangiogenic paracrine effect of DPSCs [13, 15, 16, 27]. Hypoxia priming of stem cells has thus been used as a method to increase their angiogenic potential [28–30]. Such treatment, however, only consists of exposing cells in vitro to the same stimulus as the postimplantation environment. Although it allows for earlier triggering of angiogenic properties, it might not be appropriate for increasing the extent of vessel growth. Other strategies thus need to be developed to increase the angiogenic potential of stem cells through signaling pathways distinct from, and synergistic with, the HIF pathway.

In this context, our study aimed to characterize cytokines secreted by DPSCs derived from deciduous teeth (SHED) that might explain their high proangiogenic potential and at identifying stimuli able to enhance such angiogenic properties for tissue engineering applications based on cell priming. We have demonstrated that hepatocyte growth factor (HGF) is a major regulator of DPSC-induced capillary formation, together with VEGF, and identified fibroblast growth factor-2 (FGF-2) as a potent activator of the secretion of both HGF and VEGF. We then assessed the effect of priming murine DPSCs and human SHED with either FGF-2 or hypoxia before subcutaneous implantation in mice and demonstrated that FGF-2 priming had a higher impact on angiogenesis within implanted engineered tissue constructs than did hypoxia.

Materials and Methods

Human Tooth Collection

Teeth were obtained from the Dental Department of Hôpitaux Universitaires Paris Nord Val de Seine, AP-HP, France. For cell culture, deciduous teeth were collected after trauma or after exfoliation from 3 healthy young children (3–7 years of age). For tooth section preparation, permanent third molars were obtained from young adults (18–25 years of age) after extraction according to an orthodontic treatment plan. All teeth were collected with informed and oral consent from the patients and parents according to the ethical guidelines set by the French law and with a dedicated authorization for our team (no. DC-2009-927, Cellule Bioéthique DGRI/A5, Paris, France).

Cell Culture

Culture of human pulp stem cells from exfoliated deciduous teeth (SHED) was established as previously reported [31]. In brief, after decontamination with povidone-iodine solution (Betadine; Méda Pharma, Paris, France, http://www.meda.fr), the teeth were sectioned longitudinally, and the exposed pulp tissues were collected and enzymatically digested with type I collagenase (3 mg/ml; Worthington Biochem, Freehold, NJ, http://www.worthington-biochem.com) and dispase (2 U/ml; Roche, Mannheim, Germany, http://www.roche.com). The cells were then cultured in modified Eagle's medium-α (α-MEM; Invitrogen, Grand Island, NY, http://www.thermofisher.com), supplemented with 20% fetal bovine serum (FBS; Invitrogen) and 1% penicillin/streptomycin (Invitrogen), at 37°C with 5% CO_2. The medium was refreshed after 3 days and then twice each week. The cells were detached by trypsinization at 70% confluence (0.25% trypsin EDTA solution; Sigma-Aldrich, St. Louis, MO, http://www.sigmaaldrich.com) and either frozen at −80°C or replated at a density of 10^4 cells per cm^2 in Dulbecco's modified Eagle's medium 1 g/l D-glucose (DMEM; Invitrogen) supplemented with 10% FBS (Invitrogen) and 1% penicillin/streptomycin (Invitrogen), at 37°C with 5% CO_2, with the medium refreshed twice each week. For all experiments, SHED were used between passages 2 and 4.

Human ECs from the umbilical vein were prepared as previously described [32]. They were cultivated on type I collagen in endothelial cell growth medium 2 (ECGM2; PromoCell, Heidelberg, Germany, http://www.promocell.com). The experiments were performed before passage 5. Adult normal human dermal fibroblasts were purchased from PromoCell and grown in fibroblast growth medium 2 (PromoCell).

Multicolony-derived murine pulp stem cells (mDPSCs) were obtained using a protocol adapted from Gronthos et al. [33] from the upper molars of 4-day postnatal littermate Swiss mice (Janvier Laboratories, Le Genest St. Isle, France, http://www.janvier-lab.com). The pulp tissue was digested in a solution of 3 mg/ml collagenase type I (Worthington Biochem) and 2 U/ml dispase (Roche) at 37°C for 30 minutes. Dissociated cells were plated

on 0.1% gelatin-coated dishes in α-MEM (Gibco, Grand Island, NY, http://www.thermofisher.com) supplemented with 20% FBS and 100 mg/ml streptomycin, 2.5 ng/ml FGF-2, and 10 ng/ml bone morphogenetic protein 2 and maintained at 37°C under a 5% CO_2 atmosphere. On reaching 70%–80% confluence, the cells were plated at 10^4 cells per cm^2. The number of cells necessary for the in vivo experiments was obtained after 2 passages. SHED angiogenic potential and viability were also explored by quantitative reverse transcription-polymerase chain reaction and Western blot (supplemental online data).

SHED Phenotype by Flow Cytometry

The expression of CD31, CD29, CD45, CD73, CD90, CD106, CD117, CD146, and STRO-1 was analyzed by polychromatic flow cytometry (LSRII; Becton Dickinson, Franklin Lakes, NJ, http://www.bd.com) with fluorochrome-conjugated monoclonal antibodies (BioLegend, San Diego, CA, http://www.biolegend.com; BD Biosciences, Franklin Lakes, NJ, http://www.bd.com; and eBioscience, San Diego, CA, http://www.ebioscience.com). Cells at passage 2 were detached by 4% lidocaine. BD CompBeads particles (BD Biosciences) were used to calculate the compensation of fluorescence spillover. SHED were used after 24 hours of hypoxic priming (1% O_2), 72 hours of FGF-2 treatment (10 ng/ml), 72 hours of FGF-2 treatment (10 ng/ml), including the last 24 hours in a hypoxic (1% O_2) or normoxic condition. Experiments were performed on 3 unrelated donors.

3D Migration and Tube Formation Assay

Three-dimensional fibrin gel assay was performed as previously described [34]. In brief, ECs were seeded either on Cytodex beads (GE Healthcare, Knoxville, TN, http://www.gehealthcare.com) for 24 hours before embedding in a 2.5-mg/ml fibrin gel or directly in the gel at 10^6 cells per ml. Normal dermal human fibroblasts (PromoCell) or SHED were plated on top of the gel and incubated in ECGM2 depleted for VEGF (ECGM2-ΔV). In some experiments, Cytodex beads were cultivated in SHED-conditioned medium prepared in ECGM2-ΔV. After 5–6 days, the hydrogels were fixed with 4% paraformaldehyde. Actin and nuclei were stained with Phalloidin-Alexa Fluor 488 and 4′,6-diamidino-2-phenylindole (DAPI), respectively (Invitrogen). Images were acquired with a Nikon Eclipse Ti/Roper spinning disc (Nikon, Tokyo, Japan, http://www.nikon.com). Capillary formation was analyzed using ImageJ (NIH, Bethesda, MD, http://www.imagej.nih.gov/ij).

Immunocytochemistry

Fibrin matrices were fixed with paraformaldehyde, permeabilized with 0.2% Triton-X-100, and saturated with 10% normal goat serum. They were then incubated with primary antibodies directed against CD31 (Dako, Les Ulis, France, http://www.dako-france.sas), β-catenin coupled to Alexa Fluor 647 (Cell Signaling Technology, Danvers, MA, http://www.cellsignal.com) or podocalyxin (R&D Systems, Minneapolis, MN, http://www.rndsystems.com). They were then incubated with secondary antibodies targeting mouse IgG coupled to Alexa Fluor 555 or goat IgG coupled to Alexa Fluor 488 (Invitrogen). Nuclei were stained with DAPI. Images were acquired using a Leica DMI6000-SP5 confocal microscope (Leica Microsystems, Concord, ON, Canada, http://www.leica-microsystems.com), and image analysis was performed using Imaris software (BitPlane, Zurich, Switzerland, http://www.bitplane.com).

Antibody Array and Enzyme-Linked Immunosorbent Assay

Culture supernatants were removed at each time point of culture, centrifuged, and stored at −80°C. The samples were either directly used for detection of angiogenic cytokines using antibody arrays (R&D Systems) or diluted (1/20) to be analyzed by enzyme-linked immunosorbent assay (ELISA) using the Quantikine ELISA Kit (R&D Systems) directed against human (h)VEGF and hHGF. Antibody arrays were treated as described by the provider.

Human Tooth Slice Preparation

One-millimeter-thick tooth slices were prepared from caries-free human third molars, as previously described [14, 35]. After disinfection with 70% ethanol, the teeth were transversely sectioned at the cervical region using a diamond saw blade under cooling with sterile phosphate-buffered saline (PBS; Invitrogen) to obtain 1-mm-thick dentin slices. The pulp tissue was completely removed, and the tooth slices were immersed in 0.05% sodium hypochlorite for 10 seconds and then washed with sterile PBS.

Tissue Construct Preparation for In Vivo Implantation

Tooth slices (one slice per well) were placed into 24-well cell culture-suspension plates (Cellstar; Greiner Bio-One, Basel, Switzerland, http://www.greinerbioone.com). The empty pulp chamber space was filled with 200 μl of polymerizing type I collagen gel-prepared solution (rat tail tendons obtained as previously described [36], 1 mg/ml final) containing either mDPSCs or human SHED in serum-free DMEM suspension at 1.10^6 cells per milliliter.

Surgical Procedure

Tissue constructs were implanted subcutaneously in each side of the mouse back to assess the angiogenesis capacity of the pulp cells (Agreement CEE A34.CC.003.11). In a first step, the tissue constructs seeded with mDPSCs and primed or not with 24 hours of hypoxia were implanted in Swiss mice (n = 12; Janvier Laboratories). For all experiments, a hypoxic-primed tissue construct was placed on one side of the mouse and the control tissue construct (normoxic conditions) was placed on the opposite side, each mouse being its own control. Weekly monitoring was performed using echo-Doppler and completed at 4 weeks by positron emission tomography/computed tomography PET/CT and micro-CT analysis, as described below.

In a second step, tissue constructs seeded with human SHED were tested in the same conditions in severe combined immunodeficiency (SCID) mice (n = 12; Harlan, Gannat, France), with an additional group pretreated for 24 hours with FGF-2 (10 ng/ml). Micro-CT analysis was performed 4 weeks after implantation, followed by immunohistochemistry analysis after animal sacrifice.

Ultrasound Power Doppler Analysis

Ultrasound imaging was performed using an ultrasound Biomicroscope (VEVO770; Visualsonics, Toronto, ON, Canada, http://visualsonics.com) using either a 40 MHz or 55 MHz central frequency probe (RMV-704 or RMV-708, respectively). Vascularization was assessed using either the power Doppler mode or pulsed wave Doppler mode. Tridimensional acquisitions were recorded using an integrated 3D step motor. Data were analyzed

and reconstructed in three dimensions using the VEVO770 software. The parameter analyzed was the vascular volume fraction (in percentages).

PET/CT

The distribution of the glucose analog ^{18}F-fluorodeoxyglucose (^{18}F-FDG) and a cyclic peptide ^{18}F-K5 targeting $\alpha_v\beta_1$ and $\alpha_v\beta_3$ integrins was analyzed in implanted tissue constructs (n = 9). ^{18}F-K5 was produced and purified by PETNET (Siemens Laboratory, Malvern, PA, http://www.usa.healthcare.siemens.com), as previously described [37]. The average isolated yield of ^{18}F-RGD-K5 was 26.9% $\pm$ 10.3% (decay corrected; n = 15) with an average specific activity of 9.7 $\pm$ 5.7 Ci/μmol.

PET/CT Data Acquisition

Mice were anesthetized (isoflurane/oxygen, 2.5% for induction at 0.8–1.5 l/minute and 1.5% at 400–800 ml/minute thereafter). Eight to 10 MBq of ^{18}F-FDG (n = 3) or ^{18}F-K5 (n = 6) were injected in the jugular vein. The mice were kept in standby for 1 hour after injection, and a 20-minute static PET acquisition was performed. The mice were imaged using an Inveon micro-PET/CT scanner (Siemens Healthcare, Erlangen, Germany, http://www.siemens.com). CT imaging was performed before PET acquisition for anatomical localization.

PET/CT Data Analysis

PET/CT images were analyzed by drawing volumes of interest (VOI; approximately 4 mm^3) on the implanted tissue construct area visualized on consecutive sections. For comparison, all values of radioactivity concentrations were normalized by the injected dose and expressed as a percentage of the injected dose per volume of tissue (% ID·cm^{-3}) and as the mean standardized uptake value inside each VOI (ratio of tissue radioactivity concentration at one time point, over injected activity per body weight extrapolated to the same time point).

Micro-X-Ray-CT Analysis

For angiogenesis exploration of the in-tissue constructs, the mice were anesthetized, and an intracardiac (left ventricle) injection of a contrast agent (barium chloride) was performed before scanning using an x-ray micro-CT device (Quantum FX Caliper; Life Sciences, Perkin Elmer, Waltham, MA, http://www.perkinelmer.com) hosted by the IDV Platform (EA2496; IDV Solutions, Montrouge, France, http://www.idvsolutions.com). The x-ray source was set at 90 kV and 160 μA. Tridimensional images were acquired with an isotropic voxel size of 20 μm. Full 3D high-resolution raw data were obtained by rotating both the x-ray source and the flat panel detector 360° around the sample (scanning time, 3 minutes). Tridimensional renderings were subsequently extracted from Digital Imaging and Communications in Medicine data frames using the open-source OsiriX imaging software, version 3.7.1 (distributed under LGPL license; Dr A. Rosset, Geneva, Switzerland). Quantification of the vascular density inside each tissue construct was realized using CTan Analyzer software, release 1.13.5.1 (SkyScan [now Bruker microCT], Kontich, Belgium, http://www.bruker-microct.com). A global VOI was drawn by interpolating two-dimensional regions of interest on consecutive sections to isolate tissue constructs. The obtained interpolated VOI included only 3D collagen matrices and the invading vessels into which the lumens were counter-contrasted using barium chloride. The brightness of each voxel inside the VOI was summed and distributed along a histogram. The VOI was finally segmented interactively to select barium chloride-contrasted vessels according to the threshold (a brighter range of brightness) and to eliminate background noise (a darker range of brightness). The vascular volume fraction (percentage) was the analyzed parameter.

Immunohistochemistry

Four weeks after in vivo implantation, the tissue constructs were surgically removed and fixed overnight at 4°C in 4% paraformaldehyde and then progressively demineralized in 4.13% (pH 7.3) EDTA (n = 8 per group). The tissues were embedded in paraffin and 7-μm sections prepared. Endogenous peroxidases were blocked by incubating the sections with 3% H_2O_2 at room temperature (RT) for 10 minutes. Sections were treated with 0.1% PronaseE (Sigma-Aldrich) during 10 minutes at 35°C and further incubated for 90 minutes at RT in 5% bovine serum albumin/PBS. Rabbit polyclonal antibodies for von Willebrand factor (1/800; ab6994; Abcam, Cambridge, U.K., http://wwww.abcam.com), α-smooth muscle actin (1/100; ab5694; Abcam), dentin sialoprotein (1/100; LF153; a kind gift from Larry Fisher, NIH), and calcitonin gene-retrieved peptide (1/2000; C8198; Sigma-Aldrich) were used. The sections were treated in a moist chamber overnight at 4°C and further incubated for 90 minutes with a polyclonal swine anti-rabbit immunoglobulin/horse radish peroxidase conjugate (1/1,000; Dako) as a substrate. Peroxidase visualization was obtained over 3–6 minutes in a dark chamber using 3.3′-diaminobenzidine tetrahydrochloride (Fast Dab; Sigma-Aldrich). The sections were counterstained with eosin and hematoxylin. Controls were performed by omitting the primary antibody to exclude nonspecific binding. Slices were chosen to be spaced throughout tissue constructs to count the vessels in full, lengthwise (n = 8 slices per tissue construct per antibody). Each slice was observed by microscope (Leica Microsystems Wetzlar GmbH, Wetzlar, Germany, http://www.leica-microsystems.com) ($\times$10), the reconstruction of each field was made using Microsoft Image Composite Editor software (Microsoft, Redmond, WA, http://www.research.microsoft.com), and quantification of vessel number per mm^2 and area of matrix vascularization was done using ImageJ software (NIH).

Statistical Analysis

Numerical variables are expressed as the mean $\pm$ SEM, unless otherwise indicated. The statistic analyses were performed using XLStat, version 7.5.3, software (Addinsoft, New York, NY, http://www.xlstat.com). The normality of the distribution was tested with the Shapiro-Wilk test, and the homogeneity of variance was tested with the Fisher F test. When the distribution of the data for each group respected the normality law and the variance of the groups was homogeneous, the t test for paired measures was used. When the distribution of at least one of the groups did not follow the normality law, comparisons between groups were performed with the nonparametric Kruskal-Wallis test, followed by two-by-two comparisons performed with the Mann-Whitney U test. The critical p value for statistical significance was $p < .05$.

RESULTS

SHED Have High Angiogenic Potential That Is Further Increased by Hypoxia

We first analyzed SHED' ability to promote the generation of an extended capillary network using a model that recapitulates tight

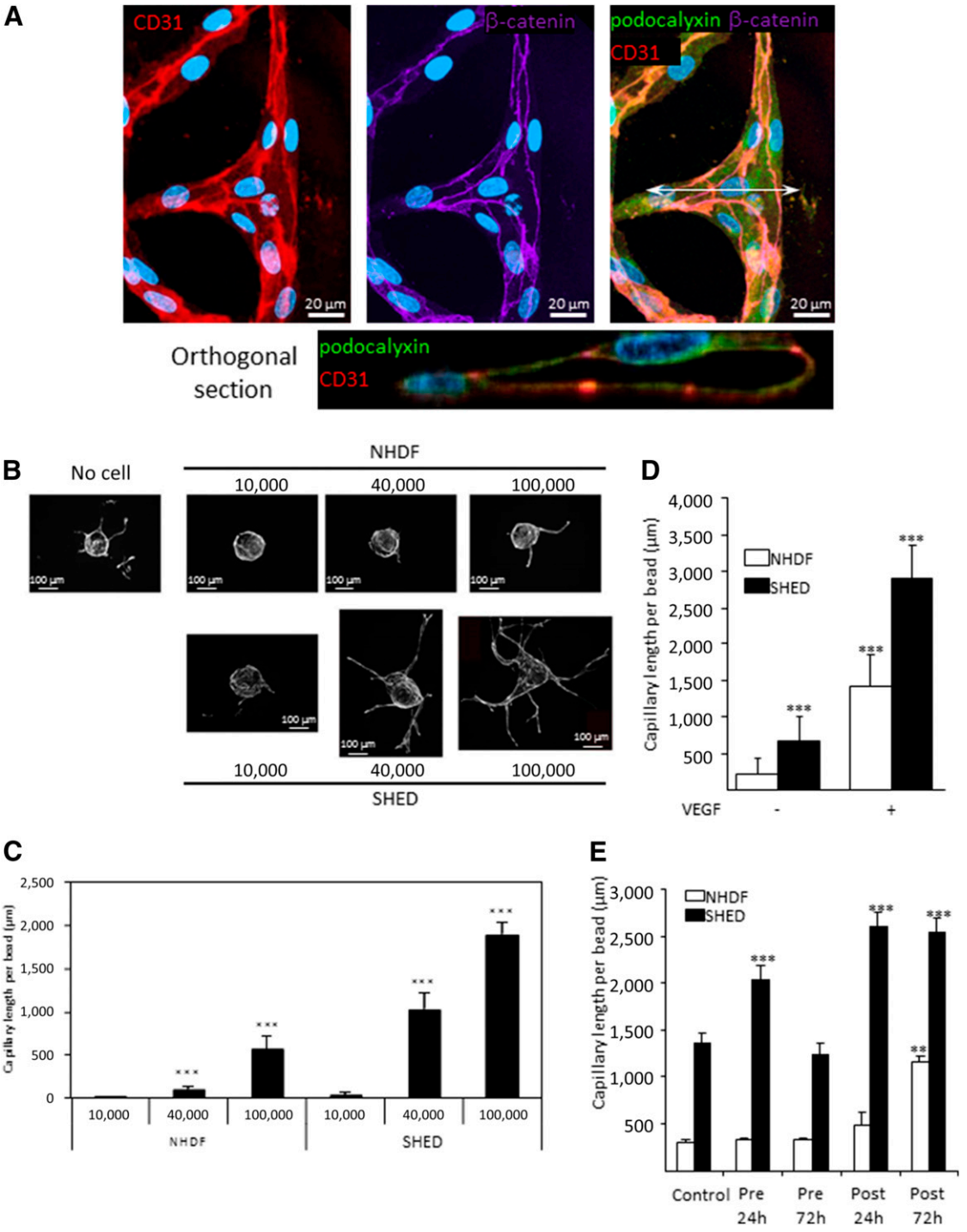

Figure 1. Formation of a three-dimensional network of endothelial capillaries induced by SHED: Positive impact of hypoxia. **(A):** Adherens junction and lumen formation by polarized endothelial cells (ECs). ECs were stained for CD31 (red), β-catenin (purple), and podocalyxin (green), and their nuclei were stained by 4′,6-diamidino-2-phenylindole (blue). Z-stack was acquired with confocal microscope and maximum projection of the stack is shown (top). Right: The overlay image. Lumen formation is illustrated in the orthogonal view of the stack along the white arrow axis (bottom: threefold enlargement). **(B, C)**: ECs were seeded on Cytodex beads and embedded in 2.5-mg/ml fibrin gel. They were maintained 5 days in endothelial cell growth medium 2 (ECGM2) depleted for VEGF, either alone or in coculture with increasing amounts of NHDF or SHED (10,000, 40,000 or 100,000 cells per well). Actin was stained using phalloidin-Alexa Fluor 488. Projections of z-stack are shown. **(D):** Capillary formation was quantitated in the six coculture conditions (***, $p < .001$). ECs embedded in fibrin gels topped with SHED were cultivated in ECGM2 supplemented or not with 5 ng/ml VEGF. **(E):** SHED were exposed to hypoxia for either 24 or 72 hours before seeding on top of the gel or at the time of embedding in the gel for 24 or 72 hours. Capillary length was measured after 5 days in culture **(D, E)**. Abbreviations: NHDF, normal human dermal fibroblast; Post, at the time of embedding in the gel for 24 or 72 hours; Pre, hypoxia for either 24 or 72 hours before seeding on top of the gel; SHED, dental pulp stem cells derived from deciduous teeth; VEGF, vascular endothelial growth factor.

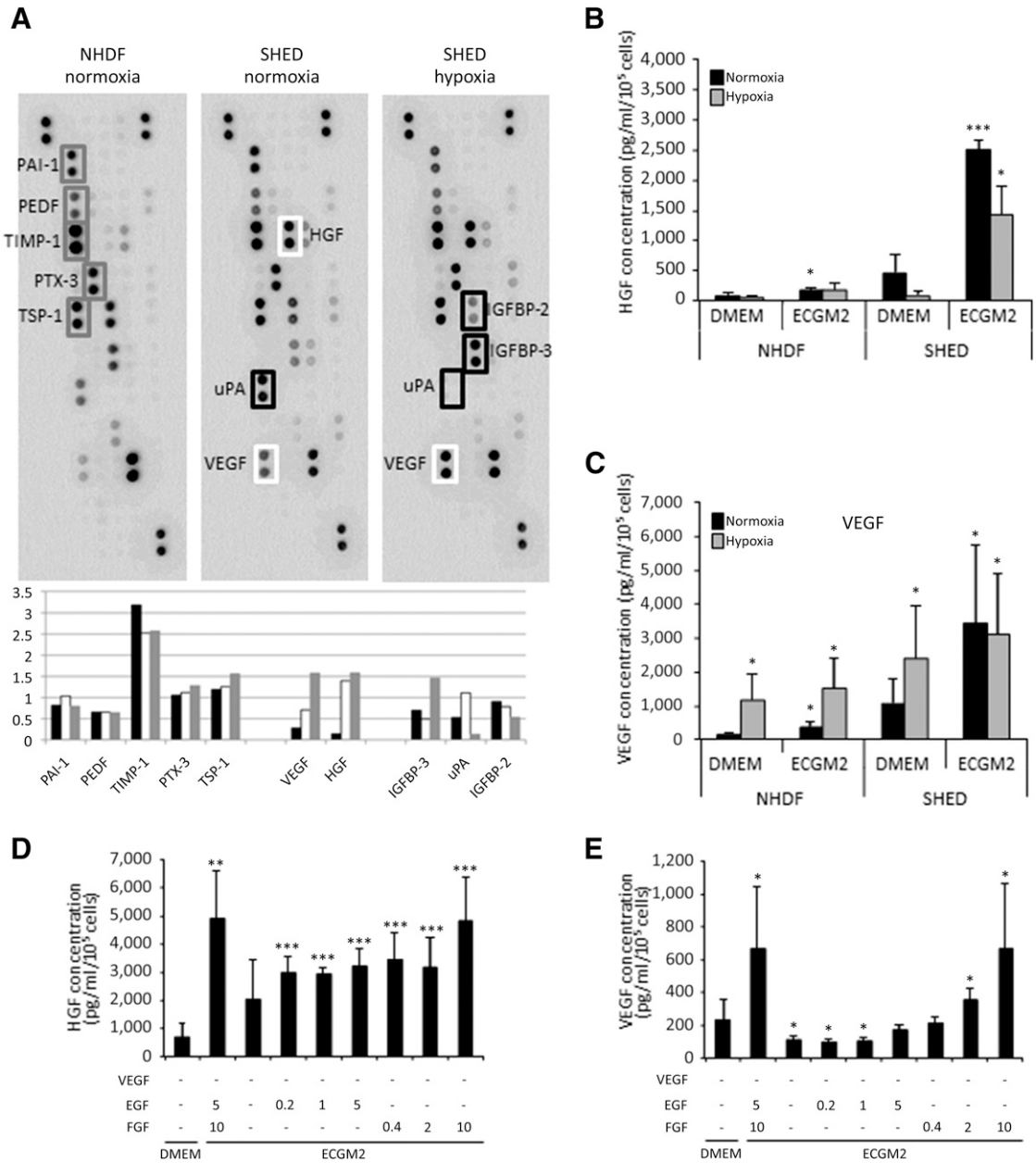

Figure 2. SHED secrete high amounts of VEGF and FGF-2. **(A)**: Overnight secretion media from NHDF or SHED cultivated in normoxia or hypoxia in ECGM2 were collected and incubated with antibody arrays. Cytokines secreted at similar levels in the three conditions are squared in gray. Cytokines upregulated in SHED in normoxia and hypoxia are squared in white. Cytokines whose pattern of secretion was not consistent with modulation of capillary growth are squared in black. Bottom: Quantification of the spots. Similar cytokine profiles were obtained using two independent donors for SHED. (**B–E):** Enzyme-linked immunosorbent assay analyses were performed for detection of HGF or VEGF in overnight medium collected after 3 days in culture. Cells were cultivated in DMEM or ECGM2 depleted for VEGF **(B, C)**. In order to identify the factors inducing VEGF and HGF, SHED were maintained in DMEM or ECGM2 depleted for VEGF, EGF, and FGF-2 and supplemented with the indicated doses of EGF or FGF-2 **(D, E)**. Mean ± SD. ∗, $p < .05$; ∗∗∗, $p < .001$. Abbreviations: DMEM, Dulbecco's modified Eagle's medium; ECGM2, endothelial cell growth medium 2; EGF, epidermal growth factor; FGF-2, fibroblast growth factor-2; HGF, hepatocyte growth factor; IGFBP, insulin-like growth factor binding protein; NHDF, normal human dermal fibroblast; PAI-1, plasminogen activator inhibitor-1; PEDF, pigment epithelium-derived factor; PTX-3, pentraxin-3; SHED, dental pulp stem cells derived from deciduous teeth; TIMP-1, tissue inhibitor of metalloproteinase-1; TSP-1, thrombospondin-1; uPA, urokinase plasminogen activator; VEGF, vascular endothelial growth factor.

control of ECM remodeling, proliferation, migration, and tubular morphogenesis. Human ECs from umbilical veins were, therefore, seeded in 3D coculture angiogenesis assays in vitro and cultured using conditioned medium from SHED (Fig. 1A). ECs could organize into an extended 3D network of capillaries, showing that SHED can sustain angiogenesis. Confocal microscopy analysis confirmed that these structures were proper capillaries. Recruitment of β-catenin at cell-cell contacts labeled for CD31 demonstrated the formation of mature adherens junctions (Fig. 1A). In addition, orthogonal reconstruction of capillaries further demonstrated lumen formation (Fig. 1A, bottom). Finally, the apical marker podocalyxin was distributed at the luminal

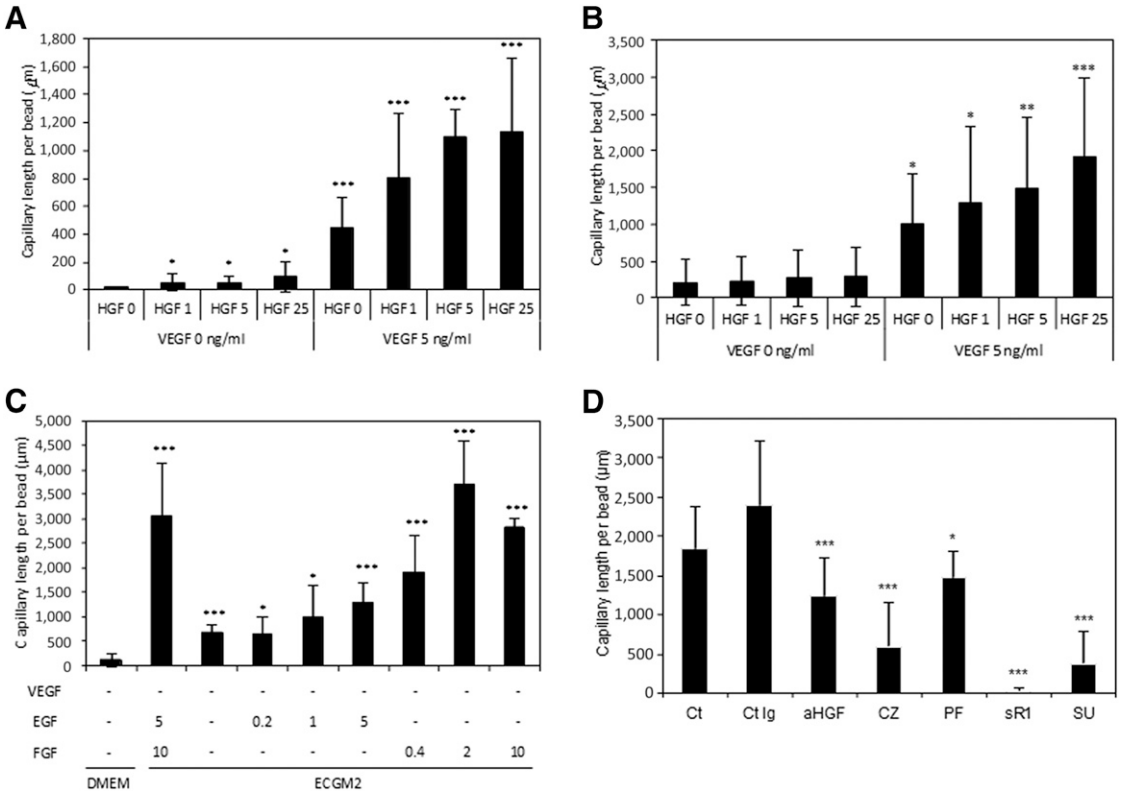

Figure 3. Capillary formation induced by SHED according to culture conditions. Endothelial cells (ECs) seeded on Cytodex beads were embedded in fibrin gels that were topped with fibroblasts and cultivated in ECGM2 depleted for VEGF or containing 5 ng/ml VEGF for 5 days **(A)**; cultivated in fibroblast-conditioned medium containing no VEGF or 5 ng/ml VEGF **(B)** (in both cases, media were supplemented with increasing amounts of HGF [1.5 or 10 ng/ml]); topped with SHED and cultivated in DMEM or in ECGM2 depleted for VEGF, EGF, and FGF-2, and supplemented with the indicated doses of EGF or FGF-2 **(C)**; or topped with SHED and cultivated in ECGM2-ΔV containing the following inhibitors of the HGF or VEGF pathway: anti-HGF or control IgG, crizotininb, PF04217903, soluble VEGF receptor 1, or sunitinib **(D)**. Capillary length per bead was measured from spinning disc acquisitions using ImageJ. Mean $\pm$ SD. *, $p < .05$; **, $p < .01$; ***, $p < .001$. Abbreviations: aHGF, anti-hepatocyte growth factor; Ct, control; Ct Ig, control IgG; CZ, crizotininb; ECGM2, endothelial cell growth medium 2; ECGM2-ΔV, ECGM2 depleted for VEGF; EGF, epidermal growth factor; FGF, fibroblast growth factor-2; HGF, hepatocyte growth factor; PF, PF04217903; SHED, dental pulp stem cells derived from deciduous teeth; SR1, soluble VEGF receptor 1; SU, sunitinib; VEGF, vascular endothelial growth factor.

side of EC, indicating the proper luminal/abluminal polarization of ECs (Fig. 1A).

In order to measure the angiogenic potential of SHED, we used an in vitro capillary assay already described using dermal fibroblasts as feeder cells and VEGF as inducer of angiogenesis [34, 38]. When ECs seeded on Cytodex beads embedded in fibrin hydrogels were maintained in ECGM2 depleted for VEGF (ECGM2-ΔV), ECs could migrate into the gel as isolated cells but could not organize into lumenized capillaries (Fig. 1B, left). Coculture with fibroblasts in the absence of VEGF resulted in inhibition of single cell migration and promoted limited formation of capillaries only at the highest fibroblast/EC ratio. In contrast, SHED could trigger an endothelial angiogenic program that resulted in extended capillary formation (Fig. 1B, 1C). The addition of 5 ng/ml VEGF to SHED further increased capillary formation. Because 5 ng/ml VEGF is the optimal dose for promoting capillary formation [39], these data suggest that SHED release additional cytokines, promoting angiogenesis (Fig. 1D). We then investigated the effect of hypoxia either by preconditioning cells (SHED or fibroblasts) using 1% O_2 before 3D coculture was initiated or by exposing them to hypoxia only during capillary growth. In both settings, hypoxia increased the angiogenic potential of SHED, but treatment of fibroblasts was either not as efficient as a preconditioning or required longer exposures (72 hours) for translating into increased angiogenesis (Fig. 1E). Twenty-four hours of preconditioning of SHED by hypoxia increased capillary formation, but 72 hours did not (Fig. 1E). Hypoxia-induced expression of VEGF followed a similar pattern, as previously described [40], although HIF stabilization and cell viability were maintained over 72 hours (supplemental online Fig. 1). Thus, our data show that SHED possess a high angiogenic potential, which can be further enhanced by hypoxia.

SHED Release High Amounts of HGF and VEGF Under Control of FGF-2 and Hypoxia

In order to identify the cytokines responsible for SHED angiogenic potential, we incubated medium from either fibroblasts, as a control, or SHED with antibody arrays targeting 55 angiogenesis-related factors overnight (Fig. 2A). Five cytokines were expressed at similar high levels by both cell types and not regulated by hypoxia (Fig. 2A, gray squares): plasminogen activator inhibitor-1 (PAI-1), tissue inhibitor of metalloproteinase-1 (TIMP-1), pigment epithelium-derived factor (PEDF), pentraxin-3, and thrombospondin-1 (TSP-1). Three additional factors were upregulated in SHED medium only (Fig. 2A): VEGF, HGF, and urokinase plasminogen activator (uPA). Hypoxia further increased VEGF secretion, although it did not affect secretion of HGF and completely inhibited that of uPA. HGF and VEGF are both potent stimulators of angiogenesis [22, 41]. Considering the limited

sensitivity of antibody arrays, we further quantified their secretion using ELISA. Fivefold higher amounts of HGF were detected in SHED secretion medium compared with fibroblasts. Although hypoxia dramatically inhibited HGF secretion by SHED in DMEM, it only slightly decreased it in ECGM2 (Fig. 2B). VEGF levels were 10-fold higher in SHED than in fibroblast medium in normoxia (Fig. 2C). Quite unexpectedly, VEGF release was not increased further by hypoxia in ECGM2-ΔV media, but it was when SHED were cultivated in serum-containing DMEM and when fibroblasts were cultivated in both media (Fig. 2C). We thus investigated the factors present in ECGM2-ΔV that could be responsible for the high HGF and VEGF secretion by SHED. Depleting epidermal growth factor (EGF) and FGF-2 suppressed VEGF secretion and inhibited HGF secretion by more than 50%. Adding back FGF-2 resulted in a dose-dependent increase in the secretion of both VEGF and HGF (Fig. 2D, 2E). In contrast, EGF had no effect, thereby demonstrating that FGF-2 was instrumental in promoting VEGF secretion by SHED. Hypoxia-induced nuclear translocation of HIF was observed using immunofluorescence, suggesting the involvement of the HIF pathway in the upregulation of VEGF. In contrast, FGF-2-induced release of VEGF did not occur through stimulation of the HIF pathway in normoxia (supplemental online Fig. 1).

HGF and VEGF Are Both Responsible for the High Angiogenic Potential of SHED

In order to assess whether HGF and VEGF were sufficient for promoting the high angiogenic potential of SHED, we incubated ECs seeded on Cytodex beads and cocultured them with fibroblasts in the absence or presence of VEGF and increasing concentrations of HGF (1–25 ng/ml). We used a low concentration of VEGF (5 ng/ml), which is the optimal dose in this assay [39]. Although HGF alone had no effect on capillary formation, it was responsible for a dose-dependent increase in capillary formation in the presence of VEGF (Fig. 3A). Similar results were obtained using conditioned media from fibroblasts (Fig. 3B), demonstrating that ECs are the actual targets of HGF in this model.

We then confirmed that increased capillary formation was mediated by stimulation of SHED by FGF-2 (Fig. 3C), through activation of HGF and VEGF pathways, using specific inhibitors (Fig. 3D). Cytokine traps (anti-HGF and soluble VEGF-R1) or inhibitors of receptor tyrosine kinase (crizotinib and PF04217903 for cMet; sunitinib for VEGF-R2) both affected SHED-induced capillary formation. Although inhibition of the HGF pathway was only partially efficient, VEGF inhibition totally abolished capillary formation. These results thus confirmed that VEGF is required for capillary formation and that HGF acts as a coinducer to further enhance the VEGF-mediated effect.

In order to determine whether hypoxic or FGF-2 priming, or the combination of both, had an effect on SHED differentiation, the expression of a series of cell surface markers associated with the mesenchymal stem cell (MSC) phenotype was investigated using flow cytometry. When cultured in normoxic conditions, SHED were positive for CD29, CD44, CD73, CD90, CD106, and CD117 and negative for CD31, CD34, and CD45 (data not shown), as expected for mesenchymal stromal cells. A small fraction of SHED (5%) was positive for Stro-1 and CD146 when cultured in normoxic conditions (Fig. 4). The fraction of Stro-1+/CD146+ progenitor cells was greatly increased after 72 hours of FGF-2 priming (10 ng/ml), 24 hours hypoxic priming (1% O_2), and 72 hours of FGF-2 priming, including the last 24 hours in hypoxia (Fig. 4). In contrast, the expression of all other markers was not affected (data not shown).

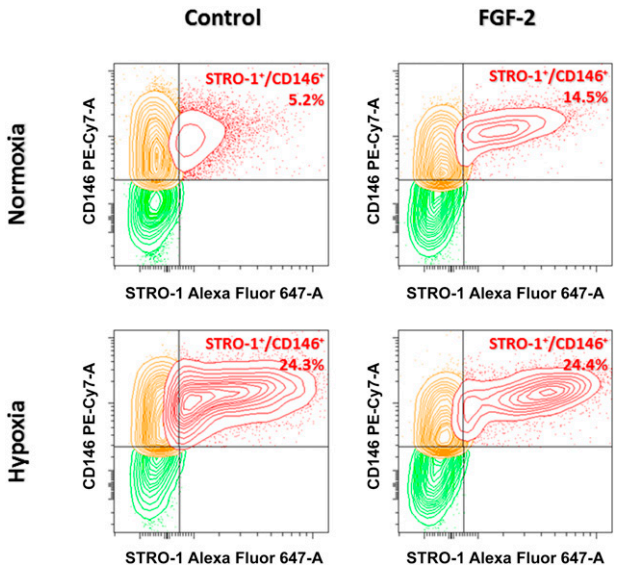

Figure 4. Characterization of dental pulp stem cells derived from deciduous teeth phenotype by flow cytometry after FGF-2 or hypoxic priming. Expression of Stro-1+ and CD146+ subpopulations was explored after 72 hours of FGF-2 treatment (10 ng/ml), 24 hours of hypoxic priming (1% O_2), 72 hours of FGF-2 treatment, including the last 24 hours under hypoxic (1% O_2) or normoxic conditions. Stro-1+/CD146+ cell fraction increased when cells were primed with hypoxia and/or FGF-2, without affecting the expression of the order markers. Abbreviation: FGF-2, fibroblast growth factor-2.

In Vivo Vascularization of Tissue Engineering Constructs Seeded With Dental Pulp Stem Cells and Primed With Hypoxia or FGF-2

The effect of FGF-2 and hypoxia priming on vascularization was investigated in vivo using a model of subcutaneous implantation of pulp cells encapsulated in a 3D collagen matrix enclosed in a tooth slice, both to hold the tissue construct and to mimic the physiological environment of the dental pulp. Because FGF-2 is necessary for generating the high amount of mouse DPSCs (mDPSCs) required for tissue construct preparation, these cells were primed with hypoxia only. We nevertheless controlled that expression of both HGF and VEGF was increased by the addition of FGF-2 to mDPSCs (supplemental online Fig. 2).

At 4 weeks, angiogenesis within the tissue constructs was studied using several complementary dynamic imaging approaches. Power Doppler ultrasound analysis indicated increased blood perfusion in the hypoxic-primed tissue constructs compared with the control side (no priming; Fig. 5A; supplemental online Movie 1). PET/CT was then used to gain insight into the cellular metabolism and angiogenesis within the constructs, using two biologically active molecules. The first was FDG, which indicates metabolic activity by virtue of local glucose uptake. The second, ^{18}F-RGD-K5, targets the RGD sequence of $\alpha_v\beta_3$ and $\alpha_v\beta_1$ integrins, which are overexpressed on activated ECs during angiogenesis. Significantly higher FDG activity and RGD-K5 binding sites were detected within the hypoxic-primed tissue constructs compared with that in the controls ($p < .05$; Fig. 5B). At the same time point, CT scan acquisitions confirmed the presence of more blood vessels in the tissue constructs that contained hypoxia-primed mDPSCs (Fig. 5C; supplemental online Movie 2). The blood vessels and vascular area were further

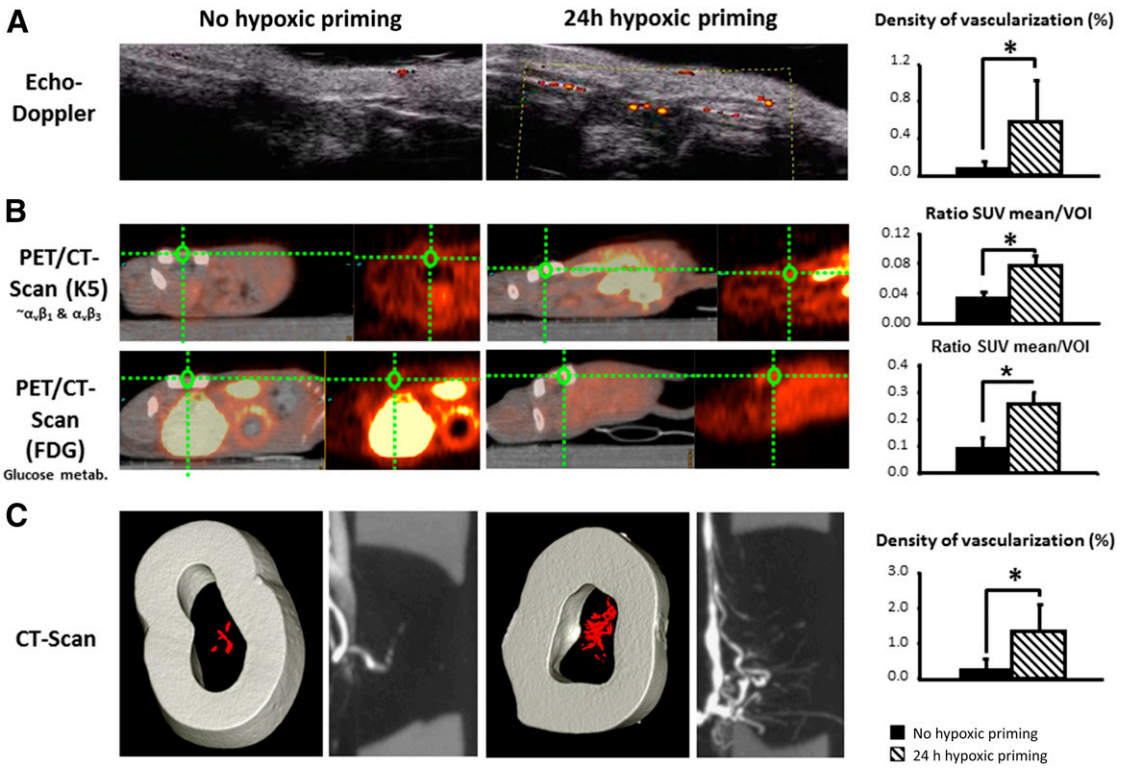

Figure 5. Vascular network and vessel visualization at 30 days in tissue constructs seeded with mouse dental pulp mesenchymal stem cells and with or without hypoxic priming. **(A):** Ultrasound acquisition. Higher blood flow (shown as red/yellow) was registered using power Doppler ultrasound imaging in the hypoxic-primed tissue constructs compared with the controls (supplemental online Movie 1). $*$, $p < .05$. **(B):** PET/CT acquisition. FDG activity (yellow) was recorded by PET associated with CT-scan acquisition and reconstructed to isolate the tissue construct (green circle) in both 24-hour hypoxic primed tissue constructs and nonprimed ones. A histogram represents the average of the data brought back to the region of interest (ROI) in both sides (0.35 ± 0.0007 to the 24-hour hypoxic primed and 0.099 ± 0.055 to the control; $*$, $p < .05$). K5 activity (yellow) was recorded by PET associated with CT scan acquisition and reconstructed to isolate the implant (green circle) in both 24-hour hypoxic primed tissue constructs and nonprimed ones. A histogram represents the average of the data brought back to the ROI in both sides (0.072 ± 0.05 to the 24-hour hypoxic primed and 0.039 ± 0.009 to the control; $*$, $p < .05$). The same observations were done to the FDG and RGD-K5, which was more binding in the 24-hour hypoxic-primed side of the mice compared with the control side ($*$, $p < .05$). **(C):** Visualization by CT scan of the vascular tree. After ultrasound and PET/CT acquisition, the mice were injected with an intravascular contrast agent to reveal the vascular tree near and inside the tissue constructs. Several reconstructions in different orientations (longitudinal and cross-sections) were performed to assess the vessels' penetration inside the matrices. Reconstructed micro-CT data vessels (red) inside and near the tissue constructs were performed showing the vessels penetrating the matrices in the group with 24-hour hypoxic priming, in contrast to the control group (supplemental online Movie 3). $*$, $p < .05$. Abbreviations: CT, computed tomography; FDG, ^{18}F-fluorodeoxyglucose; metab., metabolism; PET, positron emission tomography; SUV, standard uptake value; VOI, volume of interest.

quantified using von Willebrand factor or α-smooth muscle cell actin (α-SMA) immunohistochemistry (Fig. 6A, 6B; supplemental online Fig. 3). A significant increase in both parameters ($\times 5$ and $\times 2$, respectively) was observed in tissue constructs seeded with 24-hour hypoxia-primed mDPSCs compared with controls.

In order to distinguish the effect of FGF-2 priming from that of hypoxia, human SHED were expanded without FGF-2 and implanted in SCID mice after either FGF-2 or hypoxic priming. Micro-CT analyses showed that both FGF-2 and hypoxia priming significantly increased angiogenesis at 4 weeks after implantation ($\times 3$, $p < 10^{-6}$; Fig. 7A; supplemental online Movie 3). In SCID mice implanted with human SHED, quantification of α-SMA-positive blood vessels and total blood vessel area nonetheless confirmed the dynamic imaging observations and also revealed a significant increase in both parameters when the tissue constructs were primed with FGF-2 compared with hypoxia priming (Fig. 7B). Thus, our in vivo data indicate that FGF-2 priming is a more efficient stimulus of angiogenesis than hypoxia priming in tissue constructs seeded with DPSCs derived from deciduous teeth (SHED).

Furthermore, a sensitive innervation, which is important for the functionality of a reconstructed tissue, was observed in all the conditions using calcitonin gene-related peptide (CGRP) immunolabeling and was mainly localized around the neovessels (Fig. 6C; supplemental online Fig. 4).

Discussion

Rapid vascularization is a cornerstone in the clinical outcomes of MSC-based therapies [1]. It is thus of major importance to develop strategies aimed at both accelerating the development of new vessels and increasing the extent of blood perfusion in the tissue construct. For this purpose, we assessed in vitro priming of MSCs with FGF-2, based on our finding that this growth factor is a major inducer of both VEGF and HGF.

We have demonstrated that VEGF and HGF were upregulated in SHED culture supernatants and were responsible for their proangiogenic properties. We further showed that FGF-2 upregulated both VEGF and HGF, but only VEGF expression was increased

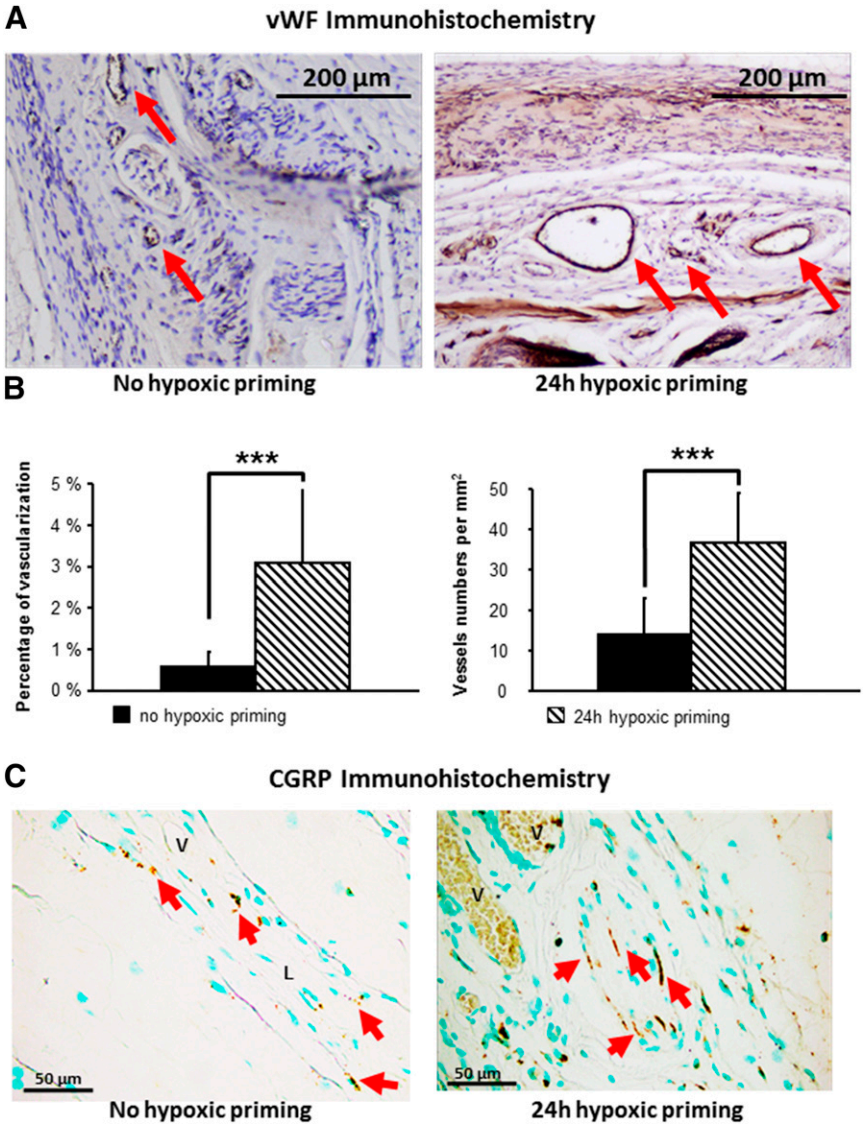

Figure 6. von Willebrand factor and CGRP staining at 30 days in tissue constructs seeded with mDPSCs with or without hypoxic priming. **(A):** vWF immunostaining. Both vessel numbers and area counting are presented in these histograms showing the difference in vascularization in the 24-hour hypoxic primed tissue constructs compared with the controls. **(B):** vWF-positive vessel numbers and vascular area counting. The number of vWF-positive vessels and their area were significantly increased in the 24-hour hypoxic primed tissue constructs when compared with controls (number: 37 ± 13 vessels/mm^2 vs. 14 ±9, ***, $p < .001$; area: 3.10 ± 1.76% vs. 0.58 ±0.38, ***, $p < .001$). **(C):** CGRP immunostaining. CGRP immunohistochemistry was then performed to investigate the sensitive innervation within the matrices. Positive immunolabeling was observed in both types of tissue constructs, especially around the neoformed vessels. Abbreviations: CGRP, calcitonin gene-related peptide; L, loaded three-dimensional collagen matrix; mDPSCs, mouse dental pulp mesenchymal stem cells; V, vessels; vWF, von Willebrand factor.

by hypoxia. HGF secretion by BMSCs and ASCs has been previously reported [42, 43]. In the case of ASCs, both regulation of HGF secretion by culture conditions and impact on vascularization were reported [44–46]. In the present study, we showed that HGF could not induce capillary formation on its own but potentiated the VEGF effects, as previously suggested [47, 48]. Secretion of PAI-1, TIMP-1, PEDF, pentraxin-3, and TSP-1 at equivalent levels to fibroblasts has also recently been described when comparing DPSCs and dental follicle precursor cells [15]. Interestingly, four of these cytokines, including TIMP-1 [49, 50], PEDF [51], pentraxin-3 [52, 53], and TSP-1 [24, 54], have already been described as anti-angiogenic, and PAI-1 is known to modulate angiogenesis in a context-dependent manner [55]. It might be hypothesized that this set of cytokines could thus be responsible for the inhibition of EC migration in 3D gel in the presence of fibroblasts or low amounts of SHED (Fig. 1A, second column). Altogether, these data demonstrated that VEGF and HGF overcome the stabilization of ECs induced by these antiangiogenic cytokines and trigger capillary growth. We thus identified HGF as a new major regulator of SHED angiogenic effects.

Capillary formation induced by SHED was strongly increased by hypoxia, as recently described for DPSCs [56, 57]. In addition to such proangiogenic effects, we have demonstrated that FGF-2 and/or hypoxia priming notably enhanced the expression of stemness markers by SHED. Such priming increased the percentage of Stro-1-positive cells, a cell membrane marker related to the

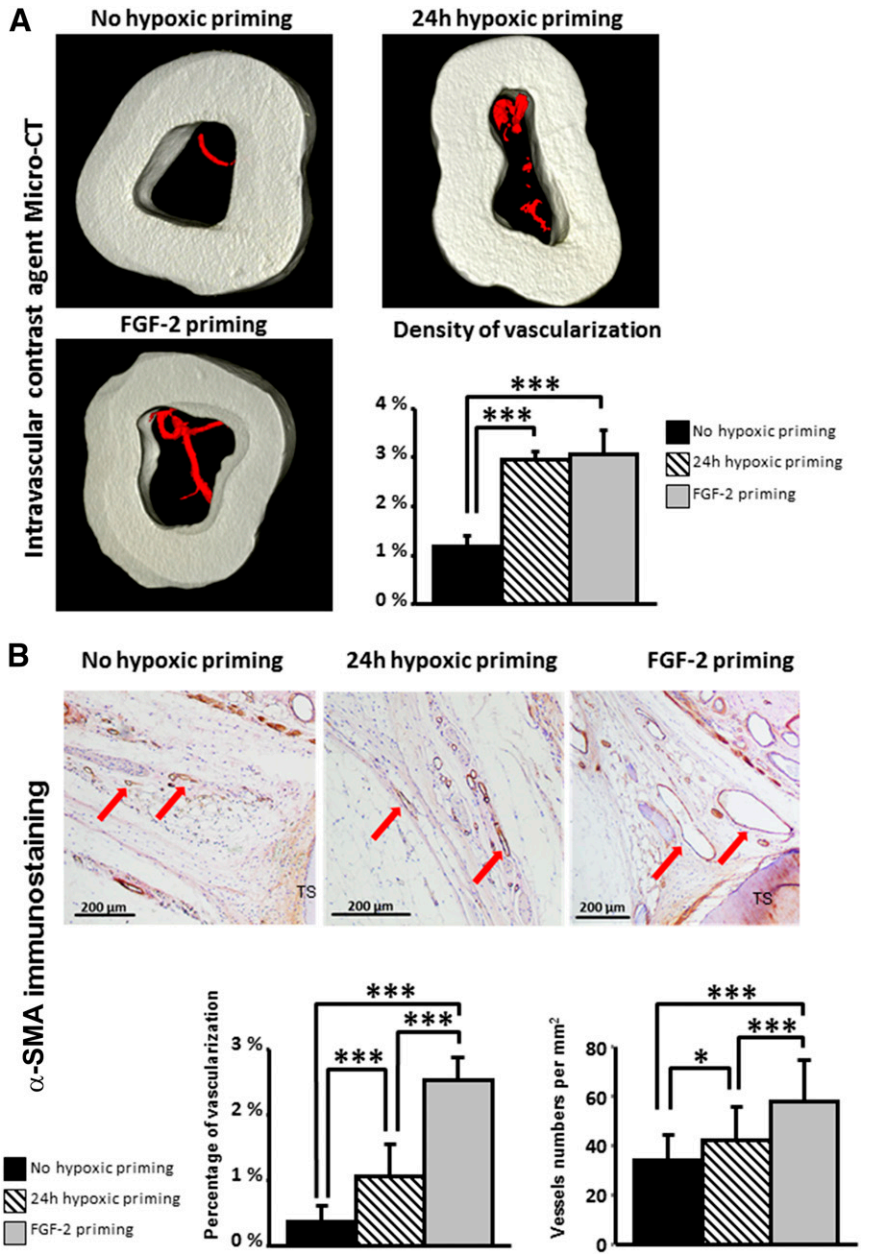

Figure 7. Vascular visualization at 30 days in tissue constructs seeded with SHED with or without hypoxic or FGF-2 priming. **(A):** Visualization by CT scan and density quantification of the vascular tree. SCID mice ($n = 12$) were injected with an intravascular contrast agent to reveal the vascular tree near and inside the tissue constructs. Reconstructed micro-CT data vessels (red) inside and near the tissue constructs were performed showing the vessels penetrating the matrices (supplemental online Movie 3). Quantification showed a significant increase in the vascular network within the tissue constructs primed by hypoxia or FGF-2 compared with controls (***, $p < 10^{-9}$ and $p < 10^{-6}$, respectively). **(B):** α-SMA immunostaining and vessel area counting. The area of α-SMA-positive vessels was significantly increased in the 24-hour hypoxic-primed tissue (1.13% $\pm$ 0.54%), and further increased in the FGF-2 primed tissue constructs (2.73% $\pm$ 0.37%) compared with control tissue constructs (0.40% $\pm$ 0.25%). The number of α-SMA-positive vessels was significantly increased in the FGF-2 primed tissue constructs (62 $\pm$ 18 vessels per mm^2) compared with the 24-hour hypoxic-primed tissue (45 $\pm$ 17 vessels per mm^2), and with control tissue constructs (36 $\pm$ 17 vessels per mm^2). *, $p < .05$; ***, $p < .001$. Abbreviations: α-SMA, α-smooth muscle actin; CT, computed tomography; FGF-2, fibroblast growth factor-2; SCID, severe combined immunodeficiency.

stemness of MSCs from numerous origins [58]. Both priming methods and their combination also increased the percentage of cells positive for CD146, a key cell adhesion molecule in EC activity and angiogenesis that has emerged as an attractive candidate for identifying genuine MSCs [58]. We detected the expression of the dentin-specific marker dentin sialoprotein [59] by the cells neighboring the human tooth slices in all the explored groups (supplemental online Fig. 4), indicating that none of the priming procedures affected postimplantation differentiation of SHED. In addition, early transient exposure to FGF-2 improved differentiation of dental progenitor cells [60].

The positive impact of priming MSCs with hypoxia had already been documented using other sources of cells [28–30]. In the present study, priming mDPSCs with hypoxia greatly improved in vivo

angiogenesis in subcutaneously implanted engineered pulp constructs, as demonstrated using independent dynamic imaging methods (micro-CT, K5-PET/CT acquisition, and echography). Furthermore, the FDG-PET/CT-positive signal indicated that the cells within the constructs were viable and metabolically active.

Conclusion

Priming SHED with FGF-2 increased more angiogenesis in the tissue constructs than did hypoxia priming. In both cases, the neovessels exhibited α-SMA labeling, indicating proper maturation of the vessels within the constructs. Quite remarkably, FGF-2-primed SHED could induce the formation of larger vessels more prone to better perfusion of the tissue construct than vessels of smaller caliber. In addition, the blood vessels were surrounded by CGRP-positive sensitive fibers, which are important for the future functionality of the implanted engineered tissue [61]. The high secretion of HGF by SHED might play an important role in tissue construct innervation, because HGF released by MSCs was recently proposed to play a major role in the recovery from experimental encephalomyelitis through improved neural cell development and remyelination [62].

The combined addition of HGF and VEGF cytokines has recently been assessed in tissue engineering studies [63, 64]. Our data suggest that priming MSC with FGF-2 before their implantation constitutes a promising approach aimed at enhancing angiogenesis in tissue constructs via VEGF and HGF release.

Acknowledgments

This work was supported by grants from the University Paris Descartes, Fondation de la Recherche Médicale for EA2496 (Grant DBS20131128438), and Plateforme d'imagerie du Vivant Paris Descartes (Grant FRM DGE20111123012), Fondation des Gueules Cassées for EA2496, and the National French Agency for Research (Grant ANR PulpCell 2014-2017). This work has also received support under the program "Investissements d'Avenir" launched by the French Government and implemented by the ANR, with the references ANR-10-LABX-54 MEMOLIFEANR-11-IDEX-0001-02 PSL Research University. N.B. and S.B. were supported by the Groupe de Reflexion sur la Recherche Cardiovasculaire and Labex Memo-Life, respectively. We thank Philippe Mailly and Nicole Quenech'Du from the Imachem imaging platform at Collège de France for image analysis, Gilles Renault (Plateforme Imagerie du Vivant Université Paris Descartes, Institut Cochin, Paris, France) for constructive comments regarding ultrasound power Doppler analysis, and Professor Michel Vidal (Faculté de Pharmacie, Université Paris Descartes, France) for helpful discussions regarding angiogenesis exploration by positron emission tomography/computed tomography scan.

Author Contributions

C.G., R.B., H.Y., J.L., J.S., N.B., S.B., A.N., M.L., B.H., L.V., D.L.-D., and C.M.: collection and/or assembly of data, final approval of manuscript; G.Y.R. and A.P.: collection and/or assembly of data, data analysis and interpretation, manuscript writing, final approval of manuscript; P.M. and S.O.V.: provision of study material or patients, final approval of manuscript; D.L.: conception and design, final approval of manuscript; A.N.: data analysis and interpretation, manuscript writing, final approval of manuscript; B.S.: collection and/or assembly of data, data analysis and interpretation, final approval of manuscript; L.M., C.C., and S.G.: conception and design, data analysis and interpretation, manuscript writing, final approval of manuscript.

Disclosure of Potential Conflicts of Interest

The authors indicated no potential conflicts of interest.

References

1 Novosel EC, Kleinhans C, Kluger PJ. Vascularization is the key challenge in tissue engineering. Adv Drug Deliv Rev 2011;63:300–311.

2 Tatullo M, Marrelli M, Shakesheff KM et al. Dental pulp stem cells: Function, isolation and applications in regenerative medicine. J Tissue Eng Regen Med 2015;9:1205–1216.

3 Gronthos S, Mankani M, Brahim J et al. Postnatal human dental pulp stem cells (DPSCs) in vitro and in vivo. Proc Natl Acad Sci USA 2000; 97:13625–13630.

4 La Noce M, Paino F, Spina A et al. Dental pulp stem cells: State of the art and suggestions for a true translation of research into therapy. J Dent 2014;42:761–768.

5 Tatullo M, Marrelli M, Paduano F. The regenerative medicine in oral and maxillofacial surgery: The most important innovations in the clinical application of mesenchymal stem cells. Int J Med Sci 2015;12:72–77.

6 Hilkens P, Meschi N, Lambrechts P et al. Dental stem cells in pulp regeneration: Near future or long road ahead? Stem Cells Dev 2015; 24:1610–1622.

7 Souron JB, Petiet A, Decup F et al. Pulp cell tracking by radionuclide imaging for dental tissue engineering. Tissue Eng Part C Methods 2014;20:188–197.

8 Menezes K, Nascimento MA, Gonçalves JP et al. Human mesenchymal cells from adipose tissue deposit laminin and promote regeneration of injured spinal cord in rats. PLoS One 2014;9:e96020.

9 Melchiorri AJ, Nguyen BN, Fisher JP. Mesenchymal stem cells: Roles and relationships in vascularization. Tissue Eng Part B Rev 2014;20: 218–228.

10 Takahashi T, Kalka C, Masuda H et al. Ischemia- and cytokine-induced mobilization of bone marrow-derived endothelial progenitor cells for neovascularization. Nat Med 1999;5:434–438.

11 Bekhite MM, Finkensieper A, Rebhan J et al. Hypoxia, leptin, and vascular endothelial growth factor stimulate vascular endothelial cell differentiation of human adipose tissue-derived stem cells. Stem Cells Dev 2014;23:333–351.

12 Iohara K, Zheng L, Wake H et al. A novel stem cell source for vasculogenesis in ischemia: Subfraction of side population cells from dental pulp. Stem Cells 2008;26: 2408–2418.

13 Bronckaers A, Hilkens P, Fanton Y et al. Angiogenic properties of human dental pulp stem cells. PLoS One 2013;8:e71104.

14 Cordeiro MM, Dong Z, Kaneko T et al. Dental pulp tissue engineering with stem cells from exfoliated deciduous teeth. J Endod 2008;34:962–969.

15 Hilkens P, Fanton Y, Martens W et al. Pro-angiogenic impact of dental stem cells in vitro and in vivo. Stem Cell Res (Amst) 2014;12: 778–790.

16 Janebodin K, Zeng Y, Buranaphatthana W et al. VEGFR2-dependent angiogenic capacity of pericyte-like dental pulp stem cells. J Dent Res 2013;92:524–531.

17 Ishizaka R, Hayashi Y, Iohara K et al. Stimulation of angiogenesis, neurogenesis and regeneration by side population cells from dental pulp. Biomaterials 2013;34: 1888–1897.

18 Sakai VT, Zhang Z, Dong Z et al. SHED differentiate into functional odontoblasts and endothelium. J Dent Res 2010;89:791–796.

19 d'Aquino R, Graziano A, Sampaolesi M et al. Human postnatal dental pulp cells co-differentiate into osteoblasts and endotheliocytes: A pivotal synergy leading to adult bone tissue formation. Cell Death Differ 2007;14:1162–1171.

20 Gandia C, Armiñan A, García-Verdugo JM et al. Human dental pulp stem cells improve left ventricular function, induce angiogenesis, and reduce infarct size in rats with acute myocardial infarction. Stem Cells 2008;26:638–645.

21 Piva E, Silva AF, Nör JE. Functionalized scaffolds to control dental pulp stem cell fate. J Endod 2014;40(suppl):S33–S40.

22 Potente M, Gerhardt H, Carmeliet P. Basic and therapeutic aspects of angiogenesis. Cell 2011;146:873–887.

23 Eilken HM, Adams RH. Dynamics of endothelial cell behavior in sprouting angiogenesis. Curr Opin Cell Biol 2010;22:617–625.

24 Germain S, Monnot C, Muller L et al. Hypoxia-driven angiogenesis: Role of tip cells and extracellular matrix scaffolding. Curr Opin Hematol 2010;17:245–251.

25 Hirota K, Semenza GL. Regulation of angiogenesis by hypoxia-inducible factor 1. Crit Rev Oncol Hematol 2006;59:15–26.

26 Gaengel K, Genové G, Armulik A et al. Endothelial-mural cell signaling in vascular development and angiogenesis. Arterioscler Thromb Vasc Biol 2009;29:630–638.

27 Dissanayaka WL, Zhan X, Zhang C et al. Coculture of dental pulp stem cells with endothelial cells enhances osteo-/odontogenic and angiogenic potential in vitro. J Endod 2012;38: 454–463.

28 Wei L, Fraser JL, Lu ZY et al. Transplantation of hypoxia preconditioned bone marrow mesenchymal stem cells enhances angiogenesis and neurogenesis after cerebral ischemia in rats. Neurobiol Dis 2012;46:635–645.

29 Zhou Y, Guan X, Wang H et al. Hypoxia induces osteogenic/angiogenic responses of bone marrow-derived mesenchymal stromal cells seeded on bone-derived scaffolds via ERK1/2 and p38 pathways. Biotechnol Bioeng 2013;110:1794–1804.

30 Hsiao ST, Lokmic Z, Peshavariya H et al. Hypoxic conditioning enhances the angiogenic paracrine activity of human adipose-derived stem cells. Stem Cells Dev 2013;22:1614–1623.

31 Miura M, Gronthos S, Zhao M et al. SHED: Stem cells from human exfoliated deciduous teeth. Proc Natl Acad Sci USA 2003;100: 5807–5812.

32 Chomel C, Cazes A, Faye C et al. Interaction of the coiled-coil domain with glycosaminoglycans protects angiopoietin-like 4 from proteolysis and regulates its antiangiogenic activity. FASEB J 2009;23:940–949.

33 Gronthos S, Arthur A, Bartold PM et al. A method to isolate and culture expand human dental pulp stem cells. Methods Mol Biol 2011;698:107–121.

34 Bignon M, Pichol-Thievend C, Hardouin J et al. Lysyl oxidase-like protein-2 regulates sprouting angiogenesis and type IV collagen assembly in the endothelial basement membrane. Blood 2011;118:3979–3989.

35 Salmon B, Bardet C, Khaddam M et al. MEPE-derived ASARM peptide inhibits odontogenic differentiation of dental pulp stem cells and impairs mineralization in tooth models of X-linked hypophosphatemia. PLoS One 2013; 8:e56749.

36 Rajan N, Habermehl J, Coté MF et al. Preparation of ready-to-use, storable and reconstituted type I collagen from rat tail tendon for tissue engineering applications. Nat Protoc 2006;1:2753–2758.

37 Kobayashi M, Murata T, Fujii N et al. A role of cytoskeletal structure of cortical cells in the gravity-regulated formation of a peg in cucumber seedlings. Adv Space Res 1999;24: 771–773.

38 Nakatsu MN, Sainson RC, Aoto JN et al. Angiogenic sprouting and capillary lumen formation modeled by human umbilical vein endothelial cells (HUVEC) in fibrin gels: the role of fibroblasts and angiopoietin-1. Microvasc Res 2003;66:102–112.

39 Nakatsu MN, Sainson RC, Perez-del-Pulgar S et al. VEGF(121) and VEGF(165) regulate blood vessel diameter through vascular endothelial growth factor receptor 2 in an in vitro angiogenesis model. Lab Invest 2003;83:1873–1885.

40 Kimura H, Weisz A, Kurashima Y et al. Hypoxia response element of the human vascular endothelial growth factor gene mediates transcriptional regulation by nitric oxide: Control of hypoxia-inducible factor-1 activity by nitric oxide. Blood 2000;95:189–197.

41 You WK, McDonald DM. The hepatocyte growth factor/c-Met signaling pathway as a therapeutic target to inhibit angiogenesis. BMB Rep 2008;41:833–839.

42 Tögel F, Weiss K, Yang Y et al. Vasculotropic, paracrine actions of infused mesenchymal stem cells are important to the recovery from acute kidney injury. Am J Physiol Renal Physiol 2007;292:F1626–F1635.

43 Rehman J, Traktuev D, Li J et al. Secretion of angiogenic and antiapoptotic factors by human adipose stromal cells. Circulation 2004; 109:1292–1298.

44 Park IS, Chung PS, Ahn JC. Enhanced angiogenic effect of adipose-derived stromal cell spheroid with low-level light therapy in hind limb ischemia mice. Biomaterials 2014;35: 9280–9289.

45 Cai L, Johnstone BH, Cook TG et al. Suppression of hepatocyte growth factor production impairs the ability of adipose-derived stem cells to promote ischemic tissue revascularization. Stem Cells 2007;25:3234–3243.

46 Boyd NL, Nunes SS, Krishnan L et al. Dissecting the role of human embryonic stem cell-derived mesenchymal cells in human umbilical vein endothelial cell network stabilization in three-dimensional environments. Tissue Eng Part A 2013;19:211–223.

47 Xin X, Yang S, Ingle G et al. Hepatocyte growth factor enhances vascular endothelial growth factor-induced angiogenesis in vitro and in vivo. Am J Pathol 2001;158:1111–1120.

48 Sulpice E, Ding S, Muscatelli-Groux B et al. Cross-talk between the VEGF-A and HGF signalling pathways in endothelial cells. Biol Cell 2009;101:525–539.

49 Thorgeirsson UP, Yoshiji H, Sinha CC et al. Breast cancer: Tumor neovasculature and the effect of tissue inhibitor of metalloproteinases-1 (TIMP-1) on angiogenesis. In Vivo 1996;10: 137–144.

50 Bloomston M, Shafii A, Zervos EE et al. TIMP-1 overexpression in pancreatic cancer attenuates tumor growth, decreases implantation and metastasis, and inhibits angiogenesis. J Surg Res 2002;102:39–44.

51 Tombran-Tink J. PEDF in angiogenic eye diseases. Curr Mol Med 2010;10:267–278.

52 Leali D, Inforzato A, Ronca R et al. Long pentraxin 3/tumor necrosis factor-stimulated gene-6 interaction: A biological rheostat for fibroblast growth factor 2-mediated angiogenesis. Arterioscler Thromb Vasc Biol 2012;32: 696–703.

53 Rusnati M, Presta M. Angiogenic growth factors interactome and drug discovery: The contribution of surface plasmon resonance. Cytokine Growth Factor Rev 2015;26: 293–310.

54 Bréchot N, Gomez E, Bignon M et al. Modulation of macrophage activation state protects tissue from necrosis during critical limb ischemia in thrombospondin-1-deficient mice. PLoS One 2008;3:e3950.

55 Bajou K, Maillard C, Jost M et al. Host-derived plasminogen activator inhibitor-1 (PAI-1) concentration is critical for in vivo tumoral angiogenesis and growth. Oncogene 2004;23:6986–6990.

56 Aranha AM, Zhang Z, Neiva KG et al. Hypoxia enhances the angiogenic potential of human dental pulp cells. J Endod 2010;36: 1633–1637.

57 Yuan C, Wang P, Zhu L et al. Coculture of stem cells from apical papilla and human umbilical vein endothelial cell under hypoxia increases the formation of three-dimensional vessel-like structures in vitro. Tissue Eng Part A 2015;21:1163–1172.

58 Lv FJ, Tuan RS, Cheung KM et al. Concise review: The surface markers and identity of human mesenchymal stem cells. Stem Cells 2014; 32:1408–1419.

59 D'Souza RN, Bronckers AL, Happonen RP et al. Developmental expression of a 53 KD dentin sialoprotein in rat tooth organs. J Histochem Cytochem 1992;40:359–366.

60 Sagomonyants K, Kalajzic I, Maye P et al. Enhanced dentinogenesis of pulp progenitors by early exposure to FGF2. J Dent Res 2015; 94:1582–1590.

61 Martens W, Sanen K, Georgiou M et al. Human dental pulp stem cells can differentiate into Schwann cells and promote and guide neurite outgrowth in an aligned tissue-engineered collagen construct in vitro. FASEB J 2014;28:1634–1643.

62 Bai L, Lennon DP, Caplan AI et al. Hepatocyte growth factor mediates mesenchymal stem cell-induced recovery in multiple sclerosis models. Nat Neurosci 2012;15:862–870.

63 Babasola IO, Rooney M, Amsden BG. Co-release of bioactive VEGF and HGF from viscous liquid poly(5-ethylene ketal ε-caprolactone-co-D,L-lactide). Mol Pharm 2013;10:4552–4559.

64 Golocheikine A, Tiriveedhi V, Angaswamy N et al. Cooperative signaling for angiogenesis and neovascularization by VEGF and HGF following islet transplantation. Transplantation 2010;90:725–731.

See www.StemCellsTM.com for supporting information available online.